DOI: 10.1002/anie.201207992

Ferroelectric Materials

Light-Induced Ferroelectricity in Bioinspired Self-Assembled Diphenylalanine Nanotubes/Microtubes**

Zhixing Gan, Xinglong Wu, Xiaobin Zhu, and Jiancang Shen*

Diphenylalanine (L-Phe-L-Phe, FF) is an interesting peptide and a promising bioinspired building block. It can readily self-assemble into various nanostructures such as nano/microtubes (NTs/MTs),[1,2] nanowires,[3–5] microcrystals,[6] and vertically aligned nanoforests.[2] Recent experiments reveal that the dipole electric field on the NTs serves as the driving force leading to the formation of hierarchical MTs.[7] Staining experiments and the external electric field-induced parallel arrangement furnish evidence of the existence of a dipole electric field in FF peptide NTs/MTs (PNTs/PMTs). Other ferroelectric and related phenomena in peptides, such as the piezoelectric effect,[8–10] second harmonic generation,[10,11] and a phase transition with a variation of symmetry, have recently been reported.[11] These results point to an intrinsic effect of the FF PNTs, namely ferroelectricity (FE).[10]

Two essential features, spontaneous polarization (SP) and a switching effect under an applied electric field, determine the FE of materials. Partial switching of the polarization along the hexagonal axis of the FF PMTs can be realized under an applied external field of 100–200 $kV\,cm^{-1}$ and higher biases will destroy the tubes.[12] The pressed PMT pellets can be switchable after annealing at about 150 °C because of a structural transition into an orthorhombic phase where electric field-induced rotation of the radial polarization component becomes possible.[13] Very recently, a piezoresponse hysteresis loop measurement revealed that the annealed PMTs exhibit radial polarization switching with a threshold voltage of about 30 V and polarization saturation at about 100 V.[14] Unfortunately, all the experiments fail to verify the predicted FE in native FF PNTs/PMTs in the direction along the tube axis. Hence, FE in FF PNTs is still a challenge.

Miniaturization of the ferroelectric crystals to the nanometer scale is strongly desirable for next-generation electronics.[15] Generally it is believed that there is a size-dependent ferroelectric effect in traditional ferroelectric materials. However, realizing low-dimensional FE is quite challenging. Although much effort has been paid to low-dimensional and nanoscale FE materials,[15–19] there have been very few reports on FE from bioinspired nanostructures.[10] Organic materials are generally flexible and their FE is readily controlled by altering their chemistry.[14] Strong and robust piezoelectric activity in bioinspired FF PNTs has been reported suggesting that FF PNTs are promising candidates as future-generation "green" nano-piezoelectrics for biomedical and medical applications.[8] The switchable SP together with the unique properties of ferroelectric materials can lead to PNTs/PMTs that have a wide range of applications but experimental verification of the predicted FE is imperative.

In FF PNTs/PMTs, direct experimental demonstration of the hysteresis loop is rather difficult because of the high coercive field of the PMTs. A change of the SP under an applied external field is an important experimental indicator to identify the possible presence of FE. In this work, the origin of the SP based on the structure of the PNTs is studied. By observing the photoluminescence (PL) spectral shift and its splitting with increasing intensity of the excitation light, we disclose the photoinduced reduction of the PNT intrinsic polarization field which implies that SP occurs at the nanoscale. The saturated polarization–electric field (P-E) loops are obtained by the action of light during the hysteresis loop measurements.

Figure 1a depicts the optical microscopy image of a cleaved PMT prepared by immersing the as-made FF PMTs in ethanol for several hours. The optical microscopic image of some PNTs stripped from the PMTs is shown in Figure 1b. The remarkable stepwise surface of the cleaved PMT confirms that the PMTs are composed of multi-NTs produced by a self-assembly process (inset),[7] indicating the presence of subnanometer crystalline regions (biological building blocks) within the NTs/MTs.[7,20–22] Our scanning electron microscopy (SEM) images also reveal that a big PMT consists of a large number of small PNTs with diameters smaller than 100 nm (Figure S1 in the Supporting Information). This implies that nanochannels form the observed NTs and finally the MTs. For simplicity, we focus on a single nanochannel structure which consists of two C(8) chains, one being a right-handed helix with a pitch of one unit cell length for each turn and the other the left-handed helix with a pitch of five unit cell lengths for each turn.[28] Thus, there is a net right-handed helix with hydrogen bonds parallel to the tube axis because of the higher density of the right-handed helical carbon chain. As shown in the lower left corner of Figure 1c, the hydrogen atom of -COOH almost becomes a proton

[*] Z. X. Gan, Prof. X. L. Wu, X. B. Zhu, J. C. Shen
National Laboratory of Solid State Microstructures and Department of Physics, Nanjing University
Nanjing, 210093 (P.R. China)
E-mail: hkxlwu@nju.edu.cn

[**] The authors sincerely thank Prof. X. M. Lv, Prof. D. Wu, and Dr. J. Su from the National Laboratory of Solid-State Microstructures, Nanjing University for their assistance in the measurement of polarization–electric field curves and Mrs. H. Xu and Mrs. J. Z. Ma from the Department of Electronic Science and Engineering, Nanjing University for the fabrication of the patterned Ni electrodes. This work was supported by the National Basic Research Program of China under grant numbers 2011CB922102 and 2013CB932901. Partial support was also from PAPD.

Supporting information for this article is available on the WWW under http://dx.doi.org/10.1002/anie.201207992.

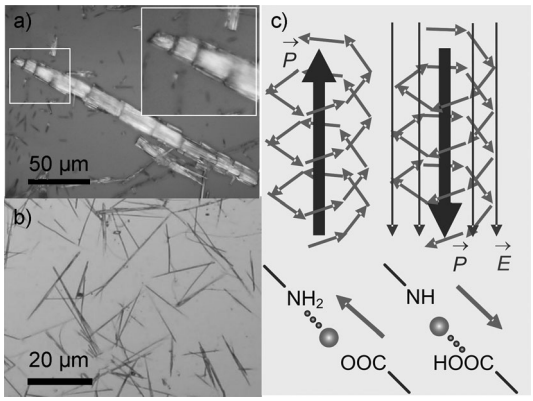

Figure 1. a) Optical microscopic image of a cleaved FF PMT. The inset shows the local enlarged area and the surface of the cleaved PMT is steplike. b) Optical microscopic image of the PNTs stripped from the PMTs. The PNTs are about 20 μm long and the diameters are smaller than 500 nm. c) Mechanism explaining the origin of the SP and the predictable FE. The gray balls represent protons, hydrogen bonds are shown as dotted lines, short arrows represent electric dipole moments of the hydrogen bonds, and long arrows mean net electric polarization in the nanochannel. For clarity, only the net helical electric dipole moments are presented. The SP in a PNT is shown on the left side whereas the right side shows that displacement of protons switches the SP under an alternative electric field.

because of the relatively high electronegativity of the oxygen atom. The proton attaches to the electronegative nitrogen forming the -NH_2···H–OOC- hydrogen bond. Because of non-overlapping positive and negative charge centers, there is a net dipolar electric field. The electric dipole moment of the hydrogen bond points from -COO^- to -NH^{3+}. So, there is a SP along the tube axis because of the net right-handed helix (the left side of Figure 1c).

Since the SP arises from orientation ordering of hydrogen bonds, the FE in the PMTs/PNTs is predictable.[19] As shown on the lower right corner of Figure 1c, when an applied electric field is antiparallel to the inherent SP, the electron of the hydrogen atom of -NH_2 shifts to the nitrogen atom and so the hydrogen atom transforms into a proton. So the -NH–H···HOOC- hydrogen bond is formed and the direction of the electric dipole moment is reversed (the right side of Figure 1c). This process can be regarded as displacement of the proton along the direction of the external field. Thus, the protons migrate and are accompanied by the switch in SP. The two essential features clearly suggest the presence of FE in the PNTs. However, since the available applied electric field is insufficient for switching,[12,14] more experiments are needed to show the possible reversal of the SP field under an applied external electric field.

Ferroelectric materials can be identified by examining the ferroelectric–paraelectric transition. So differential scanning calorimetry (DSC) was conducted on the PMTs and the results are given in Figure S2. One or two endothermic peaks are often observed at around 127 and 140 °C. To better understand the structural variation in the PMTs during the molecular transformation, Raman spectra are shown in Figure S3 (the analytical details can be found in the Supporting Information). By jointly considering the DSC result and Raman spectral modification, it can be verified that the structural transformation (SP transformation) from linear FF to cyclic FF occurs in a wide temperature interval of 120–150 °C and this transformation is not pure ferroelectric.[29] This transformation is irreversible. The ordered hydrogen bonds are destroyed when the annealing temperature is further increased. So, disappearance of SP is concomitant with the hydrogen-bond variation, suggesting that the SP in the FF PNTs/PMTs arises from an ordered hydrogen-bond network.

The SP field described above occurs in each subnanometer crystalline structure of the FF NTs[7,20–22] and thus an external electric field can principally change the SP field, that is, the quantum-confined Stark effect, which describes the separation of photogenerated carriers (electrons and holes) in a nanoscale quantum-confined structure, could be observed.[23–27] In the current FF PMTs, the light-induced Stark effect takes place in the subnanometer crystalline structure (single FF channel with an ordered hydrogen-bond network).[21,22,28] Thus, the observed step structure in the PMTs has an influence on the PNT/PMT FE because it may damage the electrical coupling between the subnanometer crystalline structures. The slope of the energy levels in a quantum emitter caused by a SP field can usually be adjusted by the applied external electric field. However, for the current FF NTs/MTs, it is a key challenge to apply a sufficient external electric field to completely reverse the SP field. Here, a light-induced field is produced by the Stark effect to reduce the SP field. As the excitation light intensity increases, the photogenerated carriers accumulate rapidly and electrons and holes are separated by the SP field simultaneously. The photogenerated carriers form a photoinduced built-in field (corresponding to an applied external filed) which adjusts the net electric field in the FF PMTs and thus changes the slope of the energy levels. As a result, the PL spectra shift with increasing excitation intensity.

To verify the above process, we prepare tubular and featherlike PMTs as well as an amorphous FF film.[7] The PL spectra obtained under different intensities of excitation light are shown in Figure 2a–c. The PL spectra (normalized) from the straight FF PMTs without divarication disclose only a single peak in each spectrum, but the peak position shifts towards the higher energy side as the excitation intensity increases (Figure 2a). For the PL spectra obtained from the featherlike PMTs, a single peak morphs into a double peak and the separation between two subbands increases with the excitation intensity (Figure 2b). With regard to the PL spectra from the amorphous film, no noticeable PL spectral shift is observed as the excitation intensity increases (Figure 2c). Figure 2d shows the PL spectra obtained from a sample thermally treated at 160 °C for 12 h. No PL spectral modification is observed when the excitation intensity changes. For the sample treated at over 160 °C, it is known that the FF PMTs transform irreversibly from linear FF to cyclic FF without polarization field.[11,29] This loss of SP and hence, the presence of the SP field in the MTs plays a crucial role in the PL band shift and splitting with increasing excitation light intensity. The SP field not only affects the PL peak energy but also the lifetime of the photogenerated charge carriers.[30,31]

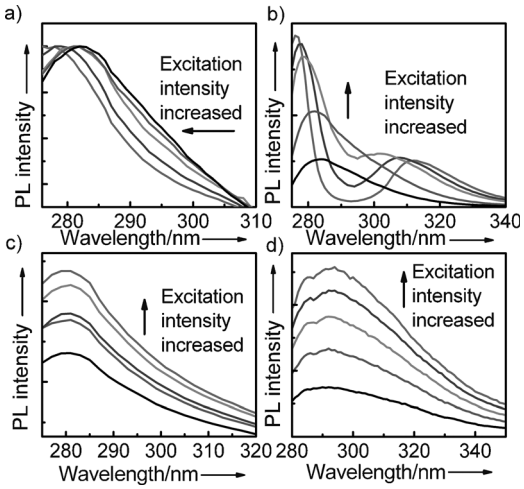

Figure 2. PL spectra of four different FF samples, taken under different excitation intensities: a) the FF PMTs without divarication (the PL intensities have been normalized to show the PL peak shift clearly), b) the featherlike FF PMTs, c) the amorphous film, and d) the thermally-treated tubular FF PMTs.

Our time-resolved PL decay measurements indicate that the fluorescence lifetimes are 17.2 and 14.7 ns for the straight PMTs and the amorphous film, respectively. This reveals that the carrier lifetime becomes longer in the presence of the SP field (Figure S4).

The light-induced change of the SP field in the FF PMTs is explained as follows. As shown in Figure 3a, the energy levels of the FF PNTs are oblique because of the SP field. When the

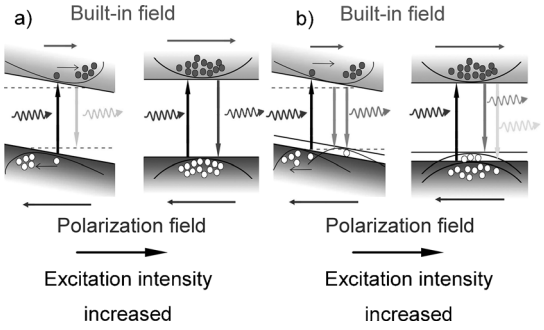

Figure 3. The mechanism explaining the PL spectral shift and splitting as the excitation intensity increases. a) For the PMTs without divarication and b) for the featherlike PMTs. The gray and empty black dots represent electrons and holes, respectively.

PMTs are excited, the photogenerated electrons and holes are separated immediately. As the excitation intensity increases, the photogenerated carriers increase in density and form a built-in electric field which is opposite to the intrinsic SP field and partially offsets the intrinsic field. Thus the net electric field decreases and the energy levels tend to be horizontal. As a result, the effective energy gap between the conduction band bottom and valence band maximum increases naturally. In the time-resolved PL result, the lower the recombination efficiency, the longer is the fluorescence lifetime.[30,31] With respect to the FF PMTs, the photogenerated electrons and holes are separated by the SP field which lowers the recombination efficiency. In an amorphous film, the SP field does not exist and the fluorescence lifetime is shorter. This is the reason why the PL band blue-shifts when the excitation increases.

Concerning the featherlike PMTs, the situation is similar but a little more complex. We have pointed out previously that when there are some water molecules in the channel cores, the symmetry of the circle with six FF molecules is destroyed thereby causing a splitting of the valence-band maximum.[32] As depicted in Figure 3b, when the photogenerated carrier density is small, the slope of the energy levels is large. The effective gap is too small to distinguish the two recombination processes by the PL spectrum. Thus, only a broad single peak is observed because of the overlapping two bands. As the excitation intensity increases, the density of the photogenerated carriers increases. This increases the built-in electric field and decreases the net electric field and energy level slope. Consequently, the single peak becomes a distinguishable double one. With increasing excitation intensity, the separation between the subpeaks gradually increases until the energy levels become horizontal and the PL separation reaches a maximum. Since the observed PL effect is related to the emitter size (nanolevel), it is obvious that the SP field occurs in the sub-nanometer crystalline unit cells in the PMTs.[7,20–22] This is the reason for such remarkable PL spectral modifications observed from the large PMTs. The current PL spectral shift and splitting with increasing excitation intensity are not a result of the water molecules added to the channel cores.[32] The excitation intensity increase only causes a gradual loss of water molecules which should decrease the separation between the two subpeaks as shown in our previous work.[32] This is inconsistent with our present results.

The switching effect of the SP under an external applied electric field is difficult to observe by a saturated hysteresis loop, but now it is possible to reverse the SP field by combining the action of sufficiently strong irradiation during the hysteresis loop measurement. Based on this idea, we measure the P-E curves of FF PMTs under irradiation of a focused Xe lamp. As shown in Figure 4a, the FF PMTs

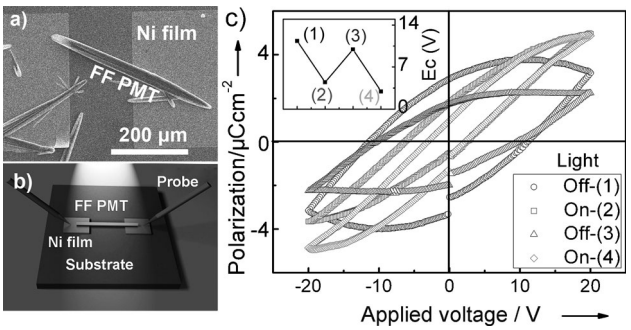

Figure 4. a) SEM image of a tubular FF PMT on the patterned electrodes. b) Acquisition of the P-E curves. c) Four P-E curves obtained from the FF PMT during the off/on switching of the light. The inset shows the light-induced coercive field variations with sequent light-off [(1) and (3)] and on [(2) and (4)] switching.

spread over an insulated coverslip with a patterned Ni film and a single PMT connects two Ni electrodes. Figure 4b shows the acquisition of the P-E curve. The obtained P-E curves are shown in Figure 4c. The curve designated "Light Off-(1)" is obtained initially in the dark and no noticeable feature of polarization saturation is observed. The "coercive field (Ec)" is about 11.3 V. After the Xe lamp is turned on, a saturated hysteresis loop appears and it has an obvious concave region (the curve named as "Light On-(2)") which is an essential feature demonstrating the ferroelectric behavior.[33] The "coercive field" decreases to about 4.28 V with the assistance of the light-induced built-in field. Here, it should be pointed out that the present "coercive field" is a synergistic effect of the applied electric field and the light-induced built-in field. The magnitude of the SP estimated from the crystallographic data is about 5.5 $\mu C\,cm^{-2}$,[7] which is in good agreement with the value reported by Heredia et al.[12] and our experimental measurement shown in Figure 4c. The ensuing photoswitching experiment shows a similar feature. After the irradiation light is turned off (the curve named as "Light Off-(3)"), the Ec value returns to about 9.88 V and decreases to about 3.02 V with further irradiation (the curve named as "Light On-(4)"). The Ec values obtained from the measurements at four different times with the light off and on are shown in the inset of Figure 4c. Because of the relative high power density of irradiation (about 2.8 $W\,cm^{-2}$), the duration of the irradiation for a single P-E curve measurement is less than 1 minute to minimize the damage of the FF PMTs caused by the intense irradiation. After long (> 10 min) irradiation, the P-E curve with the aforementioned features can no longer be observed, indicating that the PMT has been damaged.[32] To further infer the combination of MT FE with NT FE, we measured the light-induced hysteresis loops of the PMTs with different diameters and found that the P-E curve with a concave region still exists but reduces the "coercive field" and the saturated SP (Figure S5 in Supporting Information). This is because the PMTs with different sizes have a different numbers of FF nanochannels. We also measured the light-induced P-E curves of the PMTs treated at over 160 °C and no hysteresis loops were observed (Figure S6 in Supporting Information), indicating the loss of molecular polarization after thermal treatment. These results not only show that the FF PNT has FE but also indicate that it is a potential material for the detection of solar-blind-region light because of its wide bandgap and obvious response to light irradiation.

Light-induced FE is promising because light irradiation is accompanied with many interesting optical, electronic, and electric phenomena of the FF PMTs which have practical applications in various devices. For example, optical second-harmonic generation appears in the stably dispersed FF PMTs.[10,11] Molecular water sensing can be examined under light irradiation by Raman[34] and PL spectroscopy[34] of the FF PMTs. Thus, the interaction between light and FF structures is interesting and valuable in future materials science. One of the most important applications of FE is information storage. The currently light-induced FE is obviously an advantage for the biological information storage by light illumination. Though it still needs a long time to reach a real device, this work provides a scientific possibility for realizing such devices. So, we can expect that our work has practical implication in applications of PMTs.

In conclusion, we have shown that the SP in the PNTs/MTs arises from the specific hydrogen-bond network. The light-induced change of the SP field occurring in a nanoscale structure results from the interaction between the SP field and the applied external field. DSC and Raman scattering provide information about the structural transition, especially the variation in the hydrogen bonds. An obvious light-induced Stark effect is observed and it leads to an intensity reduction of the SP field. Hence, a saturated P-E loop with a concave region is obtained by combining the action of light during the hysteresis loop measurements.

Experimental Section

Fabrication and characterization details of the PMTs have been described previously.[7] The experiments were performed in a cylindrical chamber with a fixed volume of pure water inside the chamber. A fresh FF solution was prepared by dissolving the FF in 1,1,1,3,3,3-hexafluoro-2-propanol (HFIP) at a concentration of 30 $mg\,mL^{-1}$ by sonication. Afterwards, a 30 μL portion of the FF solution was placed on the slide and then kept for 60 minutes. Finally, the PMTs spreading over an insulated slide were obtained. The cleaved PMTs were obtained by immersing the as-prepared PMTs in ethanol for several hours. The heat-treated samples were obtained by keeping the as-prepared FF PMTs in an oven for 12 h at 160 °C. The DSC measurements were conducted at a heating rate of 10 $°C\,min^{-1}$ on a PerkinElmer thermal analysis system. Raman spectra were acquired on a T64000 triple micro-Raman system. SEM images were obtained on the Hitachi S-3400N II scanning electron microscope. PL and fluorescence lifetime were measured on the Edinburgh FLS-920 PL spectrometer. Typically, the excitation wavelength was 256 nm. The output slit was fixed at 8 and the excitation light intensity was controlled by modulating the input slit from 8 to 16. The patterned electrodes were fabricated by a traditional photoetching technology. The PMTs on the patterned electrodes were used for the acquisition of the P-E curves on a TF analyzer 2000HS system at an applied electric field of 500 Hz and an amplitude of 20 V. A focused 500 W Xe lamp was used to provide the required irradiation.

Received: October 3, 2012
Published online: January 10, 2013

Keywords: ferroelectricity · hydrogen bonds · peptide · phase transition

[1] L. Adler-Abramovich, D. Aronov, P. Beker, M. Yevnin, S. Stempler, L. Buzhansky, G. Rosenman, E. Gazit, *Nat. Nanotechnol.* **2009**, *4*, 849 – 854.
[2] M. Reches, E. Gazit, *Nat. Nanotechnol.* **2006**, *1*, 195 – 200.
[3] J. Ryu, C. B. Park, *Adv. Mater.* **2008**, *20*, 3754 – 3758.
[4] J. Ryu, C. B. Park, *Angew. Chem.* **2009**, *121*, 4914 – 4917; *Angew. Chem.* **2009**, *121*, 4914 – 4917.
[5] I. Yoon, J. Kim, H. Ihee, B. Kim, C. B. Park, *Angew. Chem.* **2011**, *123*, 1196 – 1199; *Angew. Chem. Int. Ed.* **2011**, *50*, 1164 – 1167.
[6] P. L. Zhu, X. H. Yan, Y. Su, Y. Yang, J. B. Li, *Chem. Eur. J.* **2010**, *16*, 3176 – 3183.
[7] M. J. Wang, L. J. Du, X. L. Wu, S. J. Xiong, P. K. Chu, *ACS Nano* **2011**, *5*, 4448 – 4454.
[8] A. Kholkin, N. Amdursky, I. Bdikin, E. Gazit, G. Rosenman, *ACS Nano* **2010**, *4*, 610 – 614.

[9] G. Rosenman, P. Beker, I. Koren, M. Yevnin, B. Bank-Srour, E. Mishinab, S. Semin, *J. Pept. Sci.* **2011**, *17*, 75 – 87.
[10] N. Amdursky, P. Beker, J. Schklovsky, E. Gazit, G. Rosenman, *Ferroelectrics* **2010**, *399*, 107 – 117.
[11] N. Amdursky, P. Beker, I. Koren, B. Bank-Srour, E. Mishina, S. Semin, T. Rasing, Y. Rosenberg, Z. Barkay, E. Gazit, G. Rosenman, *Biomacromolecules* **2011**, *12*, 1349 – 1354.
[12] A. Heredia, I. Bdikin, S. Kopyl, E. Mishina, S. Semin, A. Sigov, K. German, V. Bystrov, J. Gracio, A. L. Kholkin, *J. Phys. D* **2010**, *43*, 462001.
[13] I. Bdikin, V. Bystrov, S. Kopyl, R. P. G. Lopes, I. Delgadillo, J. Gracio, E. Mishina, A. Sigov, A. L. Kholkin, *Appl. Phys. Lett.* **2012**, *100*, 043702.
[14] I. Bdikin, V. Bystrov, I. Delgadillo, J. Gracio, S. Kopyl, M. Wojtas, E. Mishina, A. Sigov, A. L. Kholkin, *J. Appl. Phys.* **2012**, *111*, 074104.
[15] N. Nuraje, K. Su, A. Haboosheh, J. Samson, E. P. Manning, N. L. Yang, H. Matsui, *Adv. Mater.* **2006**, *18*, 807 – 811.
[16] J. Y. Son, S. W. Ryu, Y. C. Park, Y. T. Lim, Y. S. Shin, Y. H. Shin, H. M. Jang, *ACS Nano* **2010**, *4*, 7315 – 7320.
[17] S. Kim, Y. Bastani, H. D. Lu, W. P. King, S. Marder, K. H. Sandhage, A. Gruverman, E. Riedo, N. Bassiri-Gharb, *Adv. Mater.* **2011**, *23*, 3786 – 3790.
[18] H. X. Zhao, X. J. Kong, H. Li, Y. C. Jin, L. S. Long, X. C. Zeng, R. B. Huang, L. S. Zheng, *Proc. Natl. Acad. Sci. USA* **2011**, *108*, 3481 – 3486.
[19] C. F. Luo, W. Fa, J. Zhou, J. M. Dong, X. C. Zeng, *Nano Lett.* **2008**, *8*, 2607 – 2612.
[20] N. Amdursky, M. Molotskii, D. Aronov, L. Adler-Abramovich, E. Gazit, G. Rosenman, *Nano Lett.* **2009**, *9*, 3111 – 3115.
[21] C. H. Görbitz, *Chem. Commun.* **2006**, 2332 – 2334.
[22] X. L. Wu, S. J. Xiong, M. J. Wang, J. C. Shen, P. K. Chu, *Opt. Express* **2012**, *20*, 5119 – 5126.
[23] L. F. Zagonel, S. Mazzucco, M. Tence, K. March, R. Bernard, B. Laslier, G. Jacopin, M. Tchernycheva, L. Rigutti, F. H. Julien, R. Songmuang, M. Kociak, *Nano Lett.* **2011**, *11*, 568 – 573.
[24] T. Takeuchi, C. Wetzel, S. Yamaguchi, H. Sakai, H. Amano, I. Akasaki, Y. Kaneko, S. Nakagawa, Y. Yamaoka, N. Yamada, *Appl. Phys. Lett.* **1998**, *73*, 1691 – 1693.
[25] D. A. B. Miller, D. S. Chemla, T. C. Damen, A. C. Gossard, W. Wiegmann, T. H. Wood, C. A. Burrus, *Phys. Rev. Lett.* **1984**, *53*, 2173.
[26] T. Makino, Y. Segawa, A. Tsukazaki, A. Ohtomo, M. Kawasaki, *Appl. Phys. Lett.* **2008**, *93*, 121907.
[27] A. J. Bennett, R. B. Patel, J. S. Szymanska, C. A. Nicoll, I. Farrer, D. A. Ritchie, A. J. Shields, *Appl. Phys. Lett.* **2010**, *97*, 031104.
[28] C. H. Görbitz, *Chem. Eur. J.* **2001**, *7*, 5153 – 5159.
[29] A. Handelman, P. Beker, N. Amdurskyz, G. Rosenman, *Phys. Chem. Chem. Phys.* **2012**, *14*, 6391 – 6408.
[30] J. Mezyk, F. Meinardi, R. Tubino, M. Cocchi, *Appl. Phys. Lett.* **2008**, *93*, 093301.
[31] M. S. Mehata, N. Ohta, *Appl. Phys. Lett.* **2011**, *98*, 181910.
[32] M. J. Wang, S. J. Xiong, X. L. Wu, P. K. Chu, *Small* **2011**, *7*, 2801 – 2807.
[33] J. F. Scott, *J. Phys. Condens. Matter* **2008**, *20*, 021001.
[34] X. L. Wu, S. J. Xiong, M. J. Wang, J. C. Shen, P. K. Chu, *J. Phys. Chem.* **2012**, *C116*, 9793 – 9799.

